Zero offset VSP processing of fiber optic cable (DAS) and geophone array at the CaMI Field Research Station

Adriana Gordon and Don C. Lawton

ABSTRACT

Two Vertical Seismic Profiles (VSP) were acquired in May and July of 2017 at the Containment and Monitoring Institute Field Research Station (FRS) in Newell County, Alberta. These surveys were recorded using two different receiver types; a 24-level 3C geophones array and an integrated fiber optic cable (DAS and DTS). A zero-offset processing flow was completed for two shot points and an 80 m offset shot for both the fiber optic cable and geophone array. Before processing, a calibration step was necessary to estimate the exact depth for each trace in the fiber optic data set. There was an accurate result between the cross-correlation of the first and last geophone trace, a difference between 0 to 3 m or 0 to 12 traces was calculated from the calibration. After the processing flow was completed, a good match was obtained between the corridor stack of both the down-going and up-going segments of the fiber loop, as expected. A time difference of approximately 20 ms between the DAS and geophone data was also noticeable which might be caused to the difference between the signal recorded by the geophones and the fiber optic cable. A few tests for converting the DAS signals to particle velocity were evaluated and a similar calibration difference between the first and last geophone was obtained.

INTRODUCTION

As one of the objectives of the Research Field Station (FRS) is the implementation of new technologies for a better understanding and development of monitoring program for the CO_2 injection site. Fiber optic cables were permanently deployed in the observation wells, particularly the observation well 2, also called geophysical well has an integrated fiber optic cable (DAS and DTS) as well as 24-level 3C geophone array.

In this report, we will show the processing results of the DAS data recorded in May and July 2017 for several shot points. The results are compared with the geophone data set. Even though a helical-wound fiber optic cable was implemented in the observation well 2, that data set was not analyzed in this report, our main focus is on the straight fiber optic cable and the vertical component of the 3C geophone data set.

BACKGROUND

Distributed Acoustic Sensing (DAS) is a fiber optic technology that have being developing recently. DAS measurements utilizes a standard fibre optic cable instead of geophones for seismic sensing along the well. The fibre optic cable is interrogated by a special device on the surface, called an “Interrogation Unit” (IU), which measures deformations along the optical fibre caused by impinging seismic waves (Mateeva et al., 2014). The interrogator unit sends laser pulses along a fibre in the well. A tiny part of the laser light is back-scattered by random microheterogeneities naturally present in the fibre (Rayleigh scattering). Changes in the Rayleigh back-scattered pattern occur when a seismic wave deforms the fibre and these are translated into seismic measurements (Mateeva et al, 2014). By recording the time of arrival of this returning light, it can determine the position

at which each component of the returning light was generated. As this backscattered light is generated all along the fibre, the system builds up a profile of the backscattered light, and hence a dynamic profile of the strain, all along the fibre. By repeatedly firing pulses into the fibre, the changes in strain can be determined at acoustic speeds, and so, provided the system has sufficient sensitivity, the acoustic signal can be measured all along the fibre (Parker et al., 2014).

Being a recent development, DAS measurements have a number of advantages that include a low-cost acquisition once installed, is non-intrusive, has full vertical coverage, ability to use preinstalled fiber optic cables for DAS measurements. On the other hand, some of the limitations and challenges DAS VSP measurements faces involve the upfront cost of the fiber optic cable deployment, lower signal-to-noise ratio (S/N) than geophones, uncertainty in the precise locations of the DAS channels along the well and for straight fiber optic cables DAS is only sensitive to axial deformations (Mateeva et al., 2014 and Wu et al., 2015).

Two Vertical Seismic Profile (VSP) data sets were acquired this year at the Field Research Station (FRS) during the months of May and July. In this opportunity, three shot points were processed. Prior the processing, a calibration of the fiber optic data was necessary to determine the depth of the DAS channels. Determining the DAS channel depths in the fiber optic cable is usually not a problem for short and simple near-vertical wellbores, if the total length of the fiber and the precise channel spacings are known. The total length of the fiber or the exact channel spacing is not always known, and the fiber may also suffer from tortuosity along the wellbore (Wu et al., 2015). This depth calibration or tie between the fiber optic data and the geophones was performed with a cross-correlation of the fiber optic data and the first and last trace of the geophone array. Then, it was possible to identify the exact depth of the traces of the fiber optic data set and procced with the processing flow.

DAS VSP data processing largely follows the typical VSP processing sequence. However, there are aspects of the data that are specific to DAS VSP and the well trajectories that require additional processing attention (Wu et al., 2015). A standard zero-offset processing flow was modified according to the fiber optic configurations from (Bubshait, 2010) and is displayed in Figure 1.

Because the first DAS channel is not accurately known because of the surface cabling uncertainties (Wu et al., 2015), we used the geophone tie as reference point and then calculate the coordinates of DAS channels upward and downward using fixed channel spacing (Wu et al., 2015).

For VSP data with a small number of shots, such as a walkaway VSP or a small 3D VSP, the first-break time can be picked manually in a tolerable amount of time, typically on shot gathers. The advantage of manual picking is the ability of trained eyes to identify and interpolate coherent events buried in the noise with intuitive cues and constraints (Wu et al., 2015).

For typical VSP data recorded in vertical or mildly deviated wells in simple geology, downgoing wavefields are usually associated with direct arrivals and multiples and

upgoing wavefields are associated with primary reflection data. So, a simple up/down wavefield separation will sufficiently separate out the reflection data (Wu et al., 2015).

The following step is to deconvolve the data using the downgoing direct wavefield and apply it to the upgoing wavefield. The goal of deconvolution is to remove the effect of the wavelet to obtain a seismic reflectivity with is believed to be a white reflectivity series (Bubshait, 2010). Lastly, the deconvolved upgoing wavefield is the serves as input to develop the outside corridor stack mute and the corridor stack is obtained.

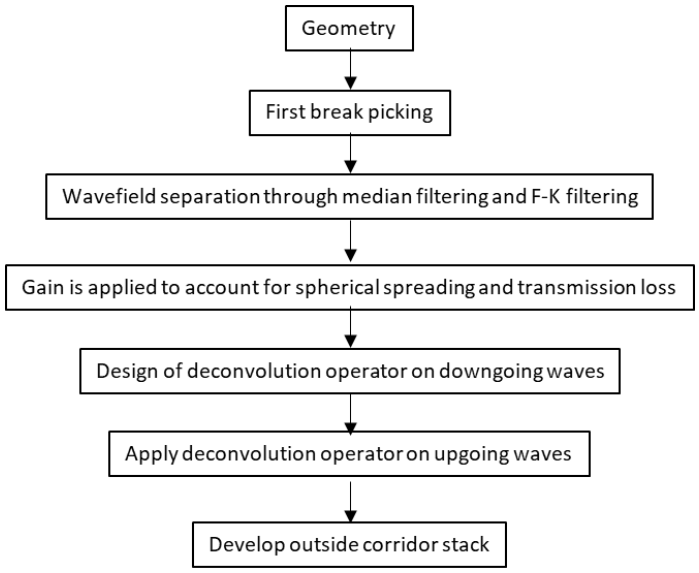

FIG. 1 Processing flow (modified from Bubshait, 2010).

DATA SETS

In May and July 2017 Vertical Seismic Profile (VSP) surveys were acquired at the Field Research Station (FRS). The location of the FRS is approximately 200 km southeast of Calgary, near the town of Brooks (Figure 1). The VSP surveys had a walk-away configuration away from the wells (NE-SW) and perpendicular (NW-SE) to the wells for the acquisition in May and a north-south and east-west direction for July survey (Figure 2). The data sets were recorded using a 24-level 3C geophone array and an integrated fiber optic cable using Distributed Acoustic Sensing technology (DAS) permanently installed in the geophysics observation well (Obs. Well 2). The source was an IVI EnviroVibe, sweeping from 10-160 Hz linearly over 16 seconds with an additional 3 seconds listening time. VISTA Desktop Seismic Data Processing Software provided by Schlumberger was used for processing the data.

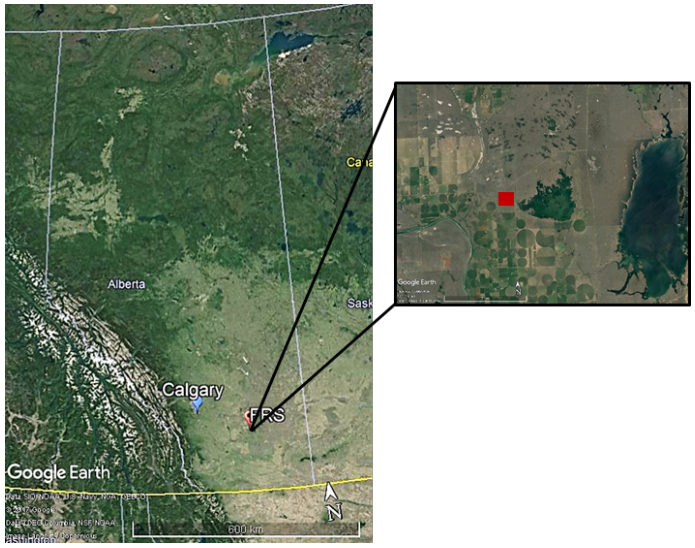

FIG. 2. FRS location marked with red box.

Figure 3 shows the survey geometry from May in red and July in blue. In this report, we focus on the shot points corresponding to zero offset at observation well 2 and an 80 m offset shot point as presented in the following table.

Table 1. Shot points processed in this report.

Date	Line	Vibe Point	Offset (m)	V. Fold
May	13	159	6.39	3
July	21	132	9.18	16
July	21	139	79.10	10

The fiber optic installation at the FRS consisted on an entire loop going from the office to the observation well 2 where straight and a helical-wound fiber optic cables were deployed in the well. Then, the fiber continues to the observation well 1 where straight fiber optic cable was deployed in the well and then it continues to a NE-SW trench as illustrated in Figure 4. An example of the fiber optic shot gathers recorded at the observation wells is displayed in Figure 5. This shot gather was recorded in July, line 21, vibe point (VP) 132, zero-offset and have a vertical fold of 16. Notice that the "V" shaped events correspond to the data recorded as the cable has a loop configuration in the well. After processing the data, it is expected to obtain similar results from each side of the "V" shaped gathers as the same energy is being recorded in each side of the fiber. This is a reliable way to QC the results and compare them to the geophone array. From this point, when we mention for a specific shot point the right or left hand side, we are referring to the part of the "V" shaped gather.

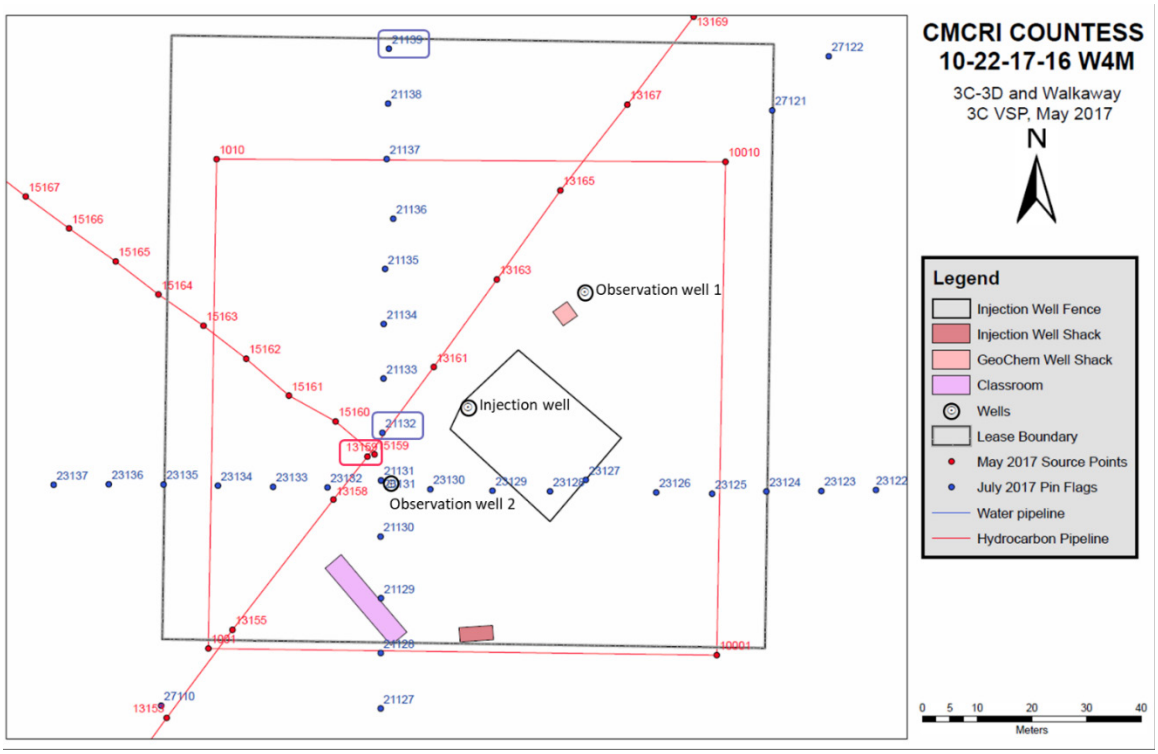

FIG. 3. Survey geometry from May in red and July in blue. The shots used in this report are highlighted with a red and blue rectangle for May and July respectively.

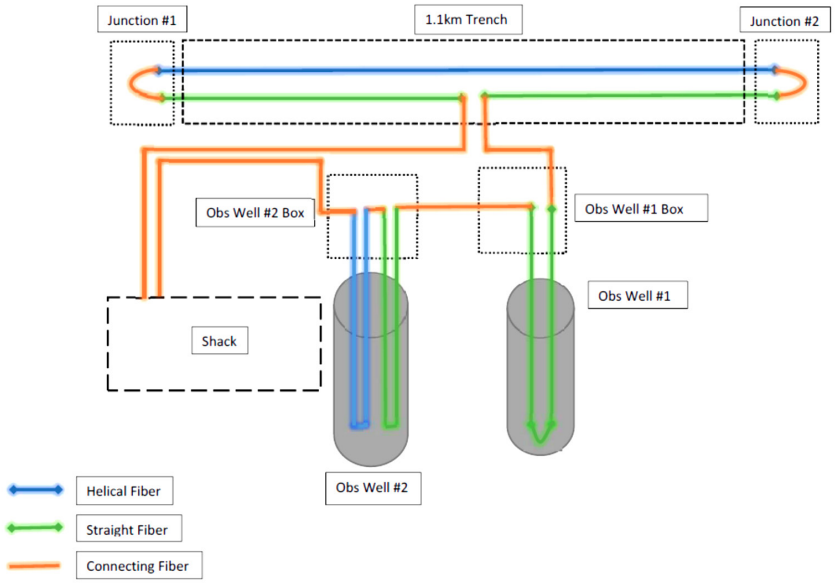

FIG. 4. Fiber optic display on site (Lawton, 2017).

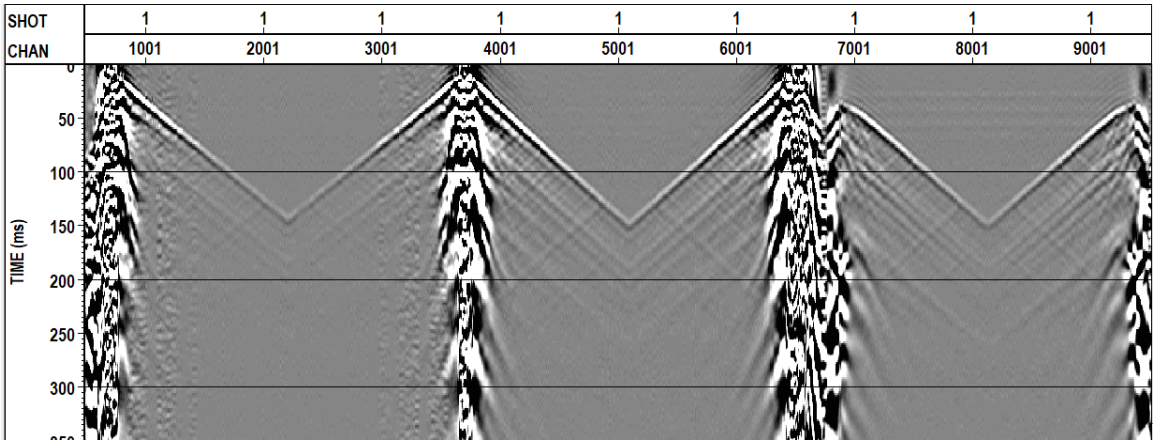

FIG. 5. Fiber optic VSP shot gathers example from July survey, shot point 132, line 21.

Data set calibration

As mentioned above, a calibration between the geophones and fiber optic data was necessary prior the processing in order to identify the depth of each trace in the fiber optic data. To quality control the data from each side of the fiber loop (left and right), a cross-correlation of both sides was performed and as expected, the result shown in Figure 6 is a straight horizontal line along the zero-lag line (250 ms). Once we verified that both sides of the fiber had a good match, we proceeded with the depth calibration. This calibration consisted on a cross-correlation of the fiber optic data with the first and last trace of the geophone array.

The first step was to truncate the length of each geophone trace to the same length as the fiber optic traces. In this case, it was truncated to 1001ms. Then, the first trace of the geophones at 194.9 m depth was duplicated 1301 times to create a gather with the same number of traces as the fiber optic gather. This was also done for the last trace of the geophones corresponding to 309.9 m depth. Each duplicated gather was cross-correlated with the fiber optic gather. From each cross-correlation, the trace of the maximum amplitude event that crossed the zero-lag line (500 ms), corresponded to the fiber optic trace that matches the depth of the first or last trace from the geophone array.

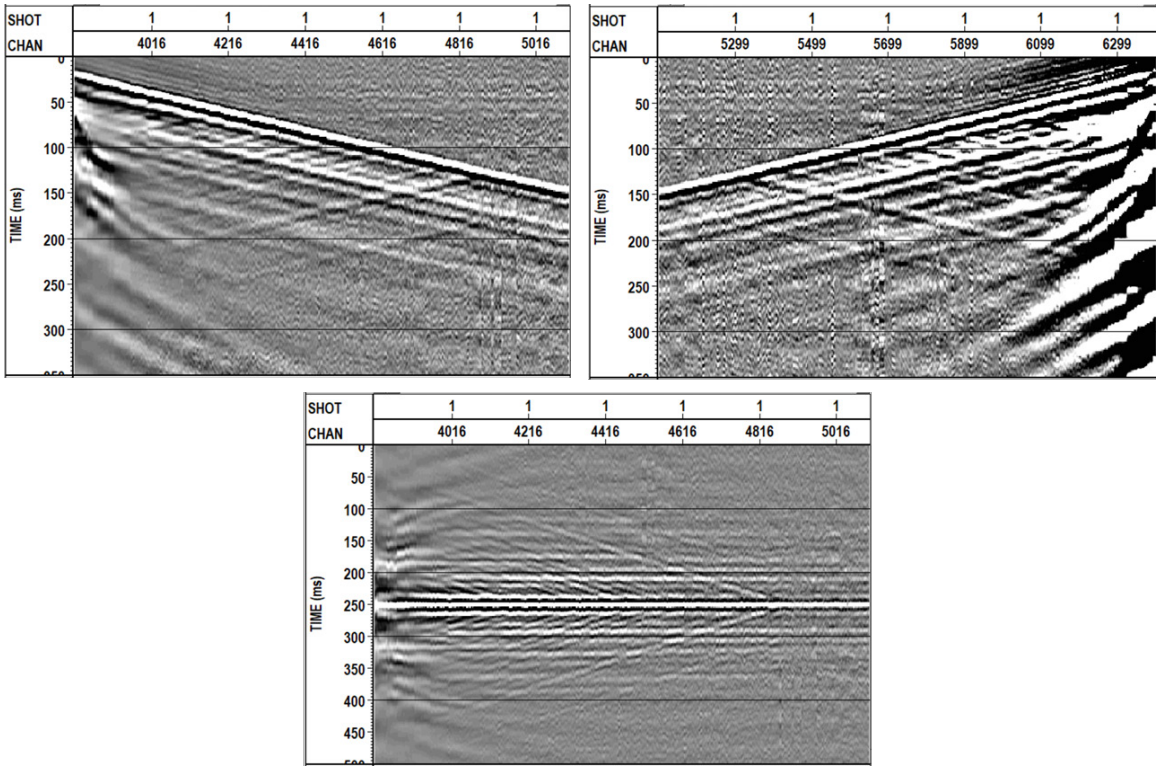

FIG. 6. DAS cross-correlation from each side of the fiber loop. Top left: left hand side of fiber loop, Top right: right hand side of fiber loop. Bottom: cross-correlation result. Shot 132, line 21 from July 2017.

Figure 7 represents an example of the calibration. The fiber optic gather corresponding to line 21, VP 132 from July is shown at the top left and the duplicated geophone trace at 194.9 m depth at the top right, and the result of the cross-correlation from this two gathers is at the bottom. A red line is highlighting the crossing point of the maximum amplitude event and the zero-lag line, in this case 500 ms, which identify the trace number that matches the depth of the first geophone (194.9 m).

After repeating the same procedure for the deepest geophone (309.9 m) the results are shown in Table 2. The difference between the depth of the first and last geophone is 115 m and knowing the 0.25 m trace spacing of the fiber optic we would expect a total of 460 traces within that depth range. In this case, the number of traces from the calibration is 456 which is an acceptable number giving the trace spacing. Figure 8 shows an example of the geophone traces at 194.9 m and 309.9 m (a and c) and the equivalent DAS trace after the depth calibration (b and d). In both cases, there is a good match between the geophone traces and the DAS traces.

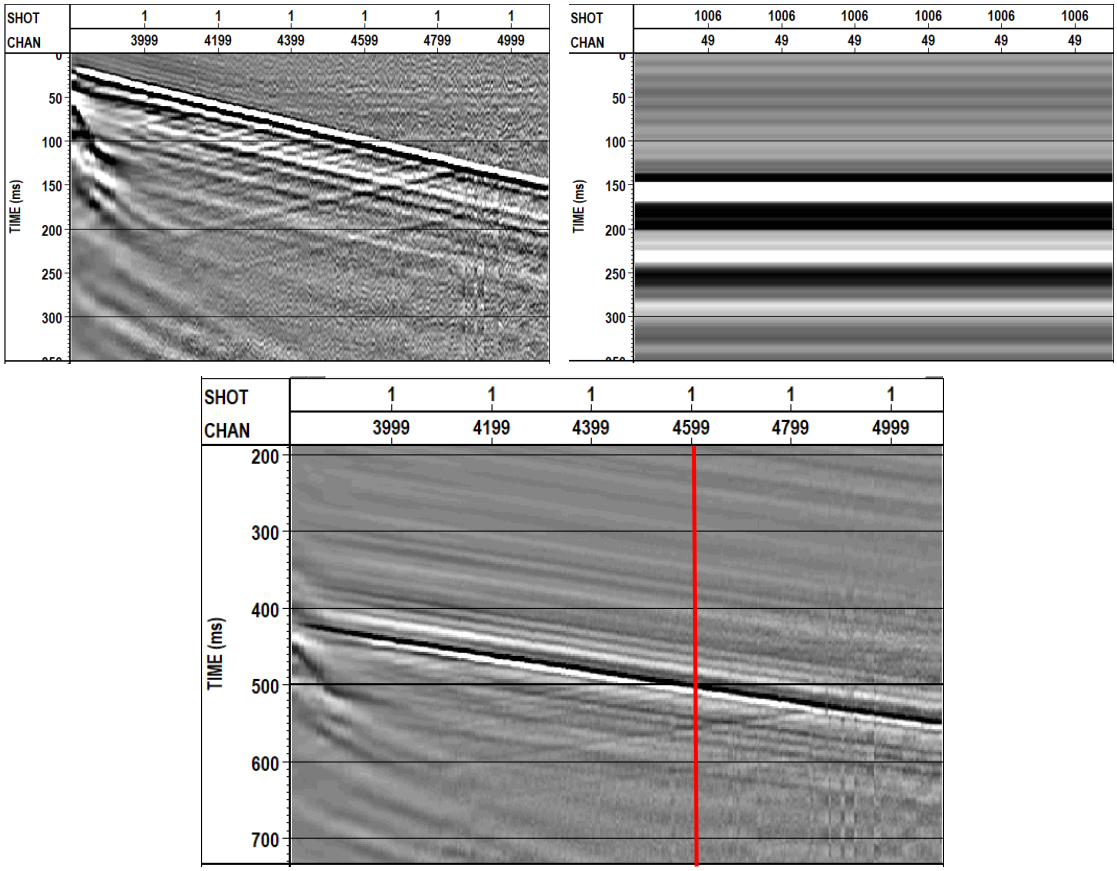

FIG. 7. Example of cross-correlation for shot point 132, line 21 from July 2017. Top left: left hand side of DAS gather, Top right: geophone trace at 194.4 m. Bottom: cross-correlation result. Red line highlight crossing of zero-lag line and maximum amplitude.

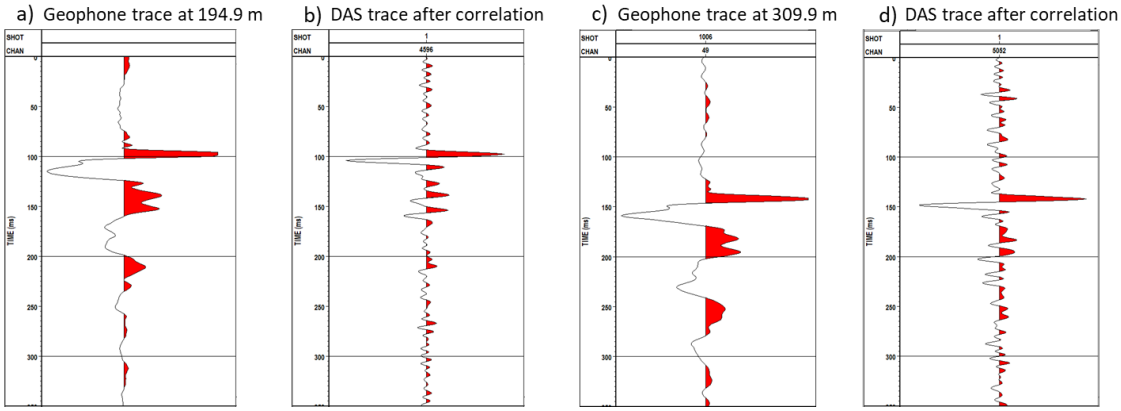

FIG. 8. Geophone and fiber trace after depth correlation. a) Geophone trace at 194.9 m. b) Fiber trace equivalent to a. c) Geophone trace at 309.9 m. d) Fiber trace equivalent to c.

Table 2. Cross-correlation result of line 21, VP 132.

	Depth (m)	Fiber optic trace	Difference
First trace geophone	194.9	797	115
Last trace geophone	309.9	1253	456

Once the depth corresponding of the first and last geophone was identified in the fiber optic gather, the calculation of the rest of the traces was done knowing the spacing of the output traces from the fibre (0.25 m). This calibration was done for the shot points on Table 1. The difference in the results between the calibration of the first and last geophone depth vary from 0 to 3 meters, equivalent to 0-12 traces and the largest difference was obtained for the 80 m offset source point. Since the difference was relatively small, the calibration of the first geophone was taken as starting point for the calculation of the depth for each trace in the DAS data. After this calibration step, the geometry was updated and the processing flow could proceed.

PROCESSING

The processing flow described previously was performed for the fiber optic and geophone gathers corresponding to the shot points in Table 1. An example of each step in the flow will be displayed in this section for both data sets. However, only the final step of the processing flow corresponding to the outside corridor stack will be shown for other two shot points.

The step by step display corresponds to the zero-offset shot point 132, line 21 from July. Generally, the left hand side of figures will show the fibre outcome and the right hand side will show the geophone outcome for comparison. Figure 9 is showing the first break picked and figure 10 shows the interval velocities calculated, that essentially are a 1D velocity model that will be used later in walkaway VSP processing (Bubshait, 2010).

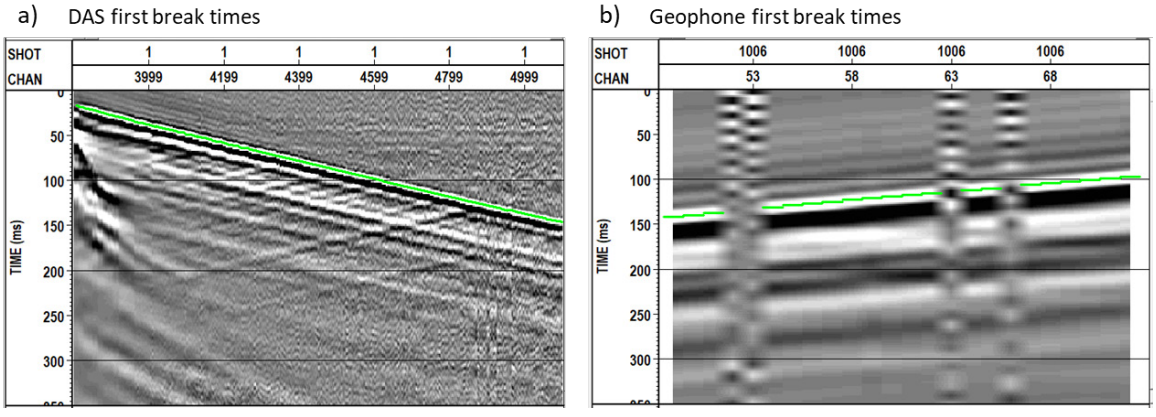

FIG. 9. First break picks of shot point 132, line 21 from July 2017.

In Figure 10.a, the first break times are plotted with respect to depth in blue and Figure 10.b shows the interval velocities in red and RMS velocities in blue. Given the high density of traces on the DAS data set and the precision of the first break times, the interval velocity profile is noisy and does not present a block shape as expected because of the small output trace spacing (0.25 m). One way to account for this effect will be to apply a median filter to the first break times and resample the velocity profile. This approach will be addressed as part of the future work as the velocity model will be necessary for the walk-away processing flow and is not our current focus for this report. On the other hand, there is a good block shape in the interval velocities of the geophone data.

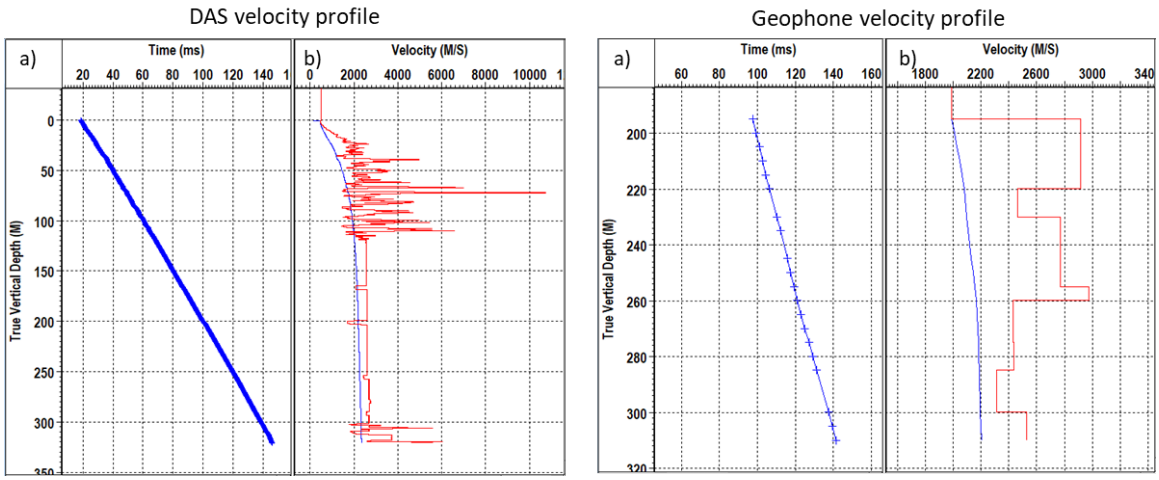

FIG. 10. Velocity profile obtained from first break picks. a) first break times versus depth in blue. b) interval velocity (red) and RMS velocity (blue).

After the first break picking and the velocity profile display, the following step was to apply a median filter for separating the upgoing and downgoing wave fields. For the fiber optic data, a median filter of 91 samples corresponding to 22.75 m length. For the geophone data, a median filter of 5 samples corresponding to 25 m length. These two values vary considerately due to the difference in the number of traces and trace spacing of the two data sets. Figure 11 represents the data after a flattening function was applied, before the median filter. Figures 12 and 13 display the downgoing and upgoing wavefield respectively after application of the median filter.

Both the downgoing and upgoing wavefields are noticeable in Figures 9 and 11. The median filter had outcomes separating the downgoing wavefield as shown in Figure 12 for both data sets. Nevertheless, the upgoing wavefield of DAS data in Figure 13 still includes noticeable downgoing events. These events of low frequency were separated from the upgoing wavefield using a F-K filter. Figure 14 shows the F-K filter design and Figure 15 is the resulting upgoing wavefield after application of the F-K filter.

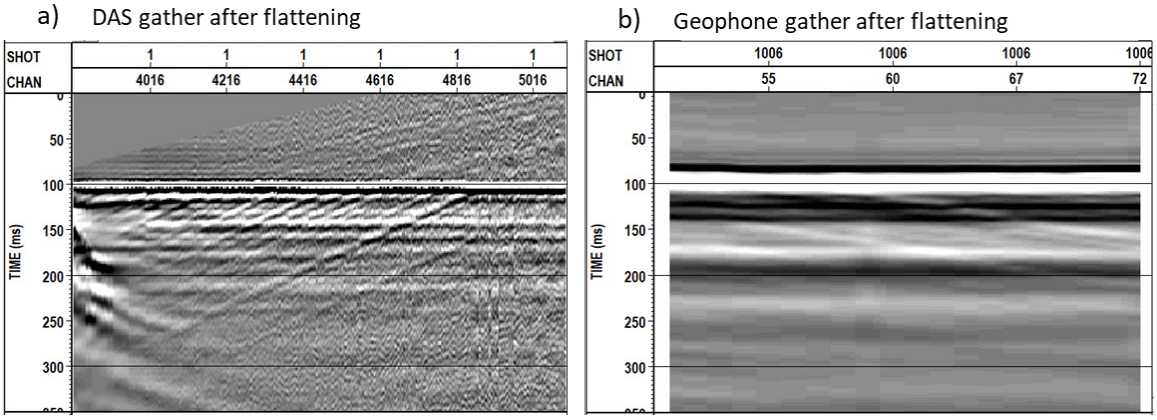

FIG. 11. Shot gather after flattening; Shot point 132, line 21 from July 2017.

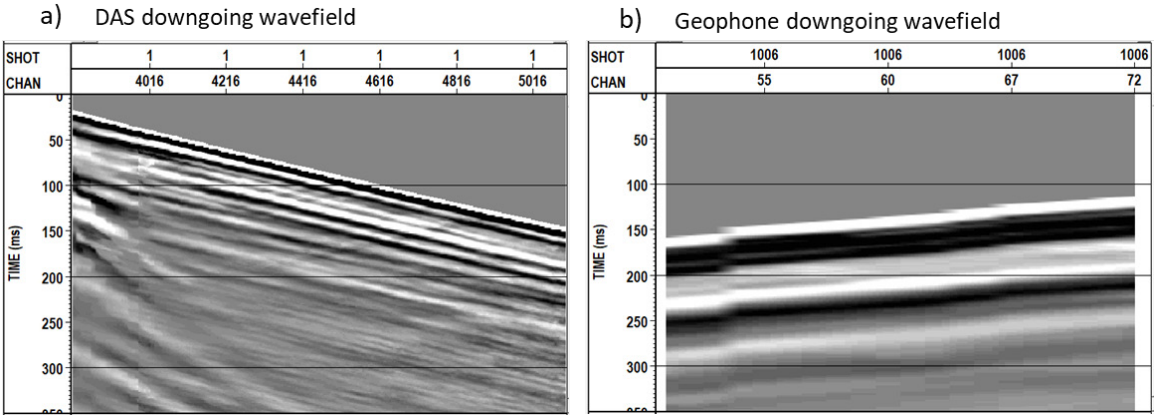

FIG. 12. Downgoing wavefield after median filtering. Shot point 132, line 21 from July 2017.

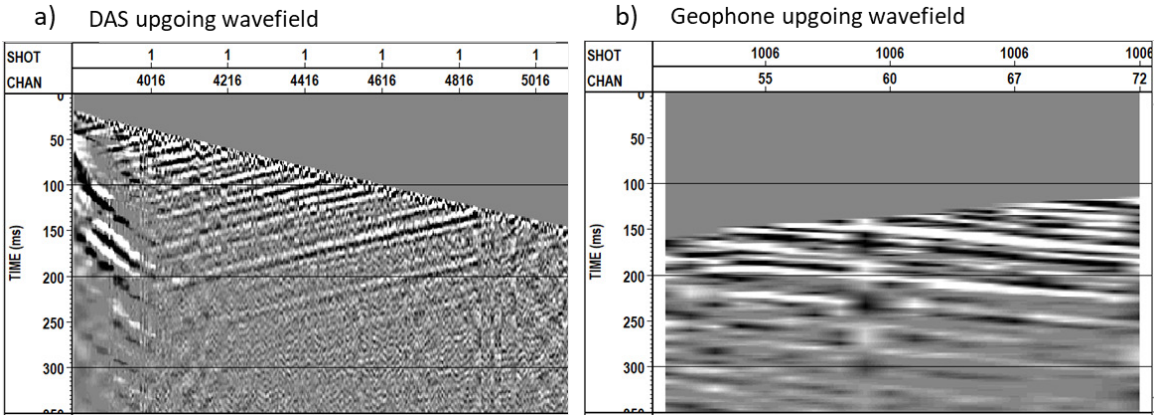

FIG. 13. Upgoing wavefield after median filtering. Shot point 132, line 21 from July 2017.

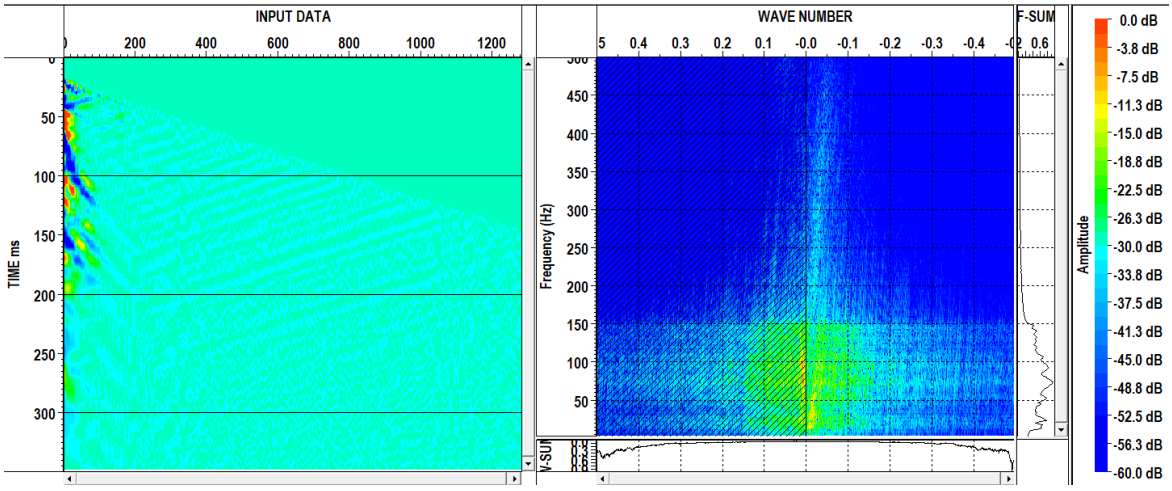

FIG. 14. F-K filter design for wavefield separation.

The next step was to create a deconvolution operator and apply it to the upgoing wavefield. Figures 16 and 17 represent the downgoing and upgoing wavefield after deconvolution, where the events are sharper, better defined and no multiples are evident.

An amplitude spectrum analysis of the upgoing wavefield was done before and after deconvolution, the result is displayed in Figure 18. For the DAS data set the frequency range of the sweep is noticeable up to 150 Hz before deconvolution, for the geophone data set is harder to notice the complete frequency range of the sweep. After deconvolution, both spectrums show an average white reflectivity in the same range of frequencies.

The final step in the work flow was to develop the outside corridor stack. Figure 19 shows the outside corridor stack mute of 50 ms obtained and Figure 20 display the outside corridor stack.

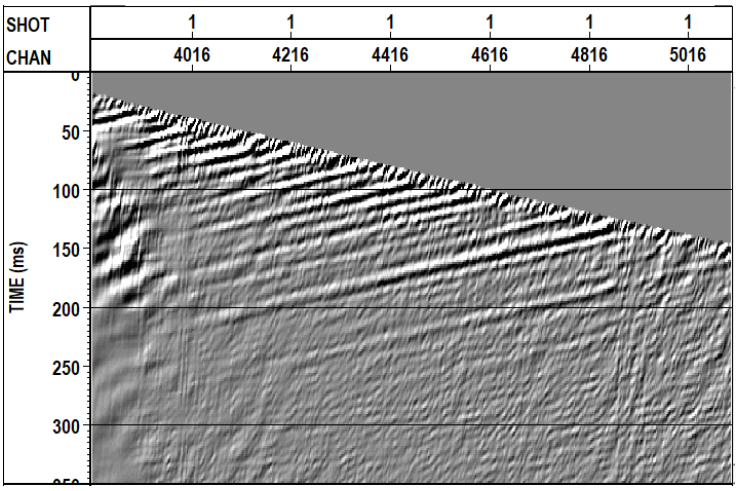

FIG. 15. Upgoing wavefield after application of the F-K filter. Shot point 132, line 21, July 2017.

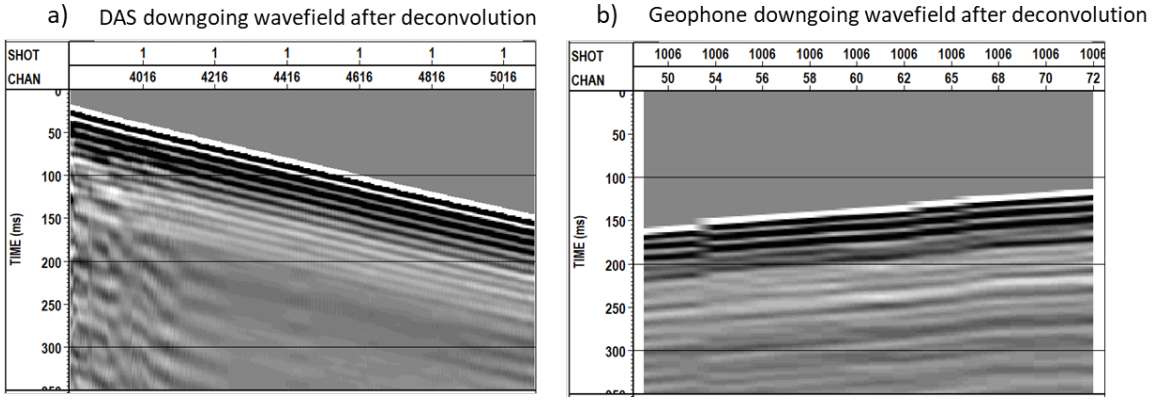

FIG. 16. Downgoing wavefield after deconvolution.

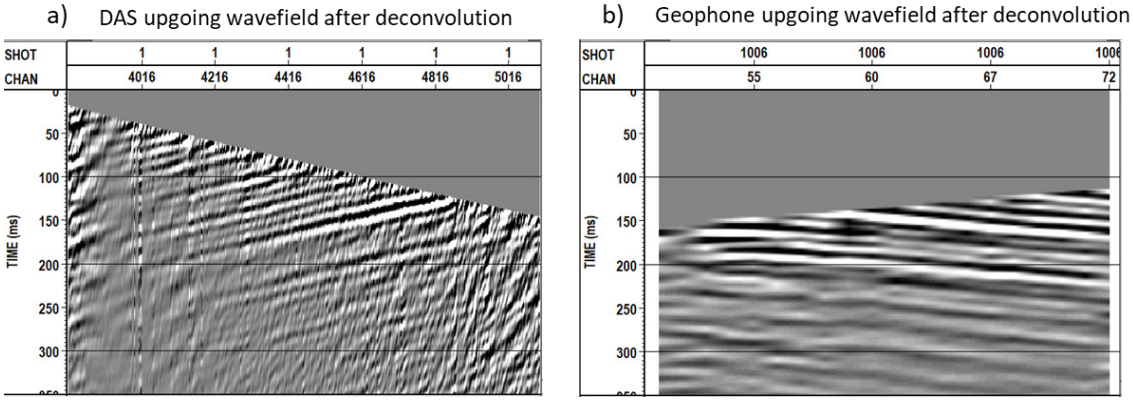

FIG. 17. Upgoing wavefield after deconvolution.

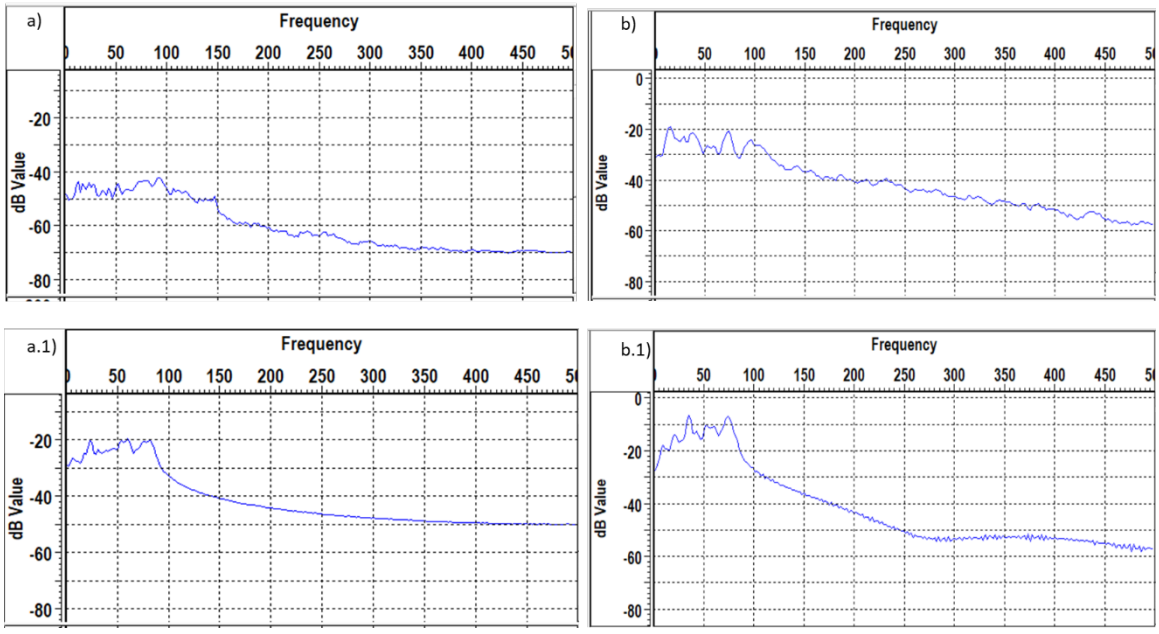

FIG. 18. Amplitude spectrum of the upgoing wavefield. a) Before deconvolution (Figure 14). b) After deconvolution (Figure 16).

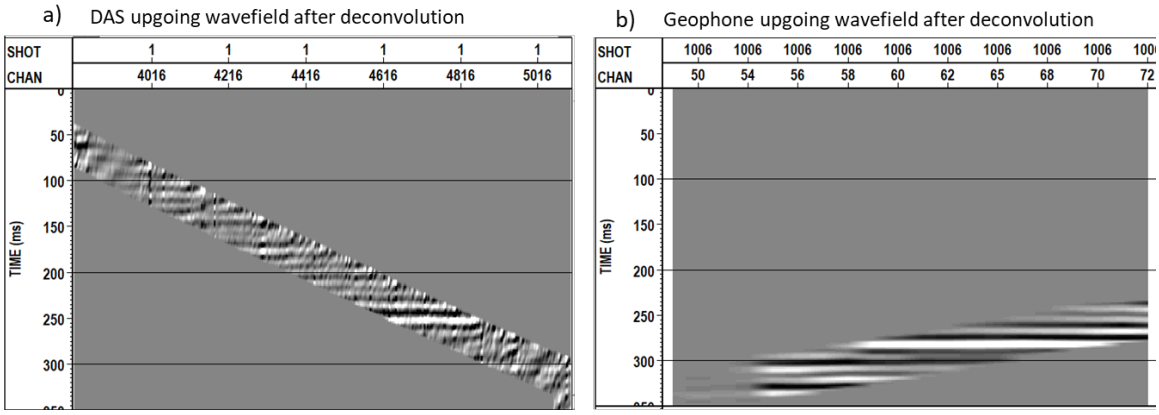

FIG. 19. Outside corridor stack mute. Shot point 132, line 21, July 2017.

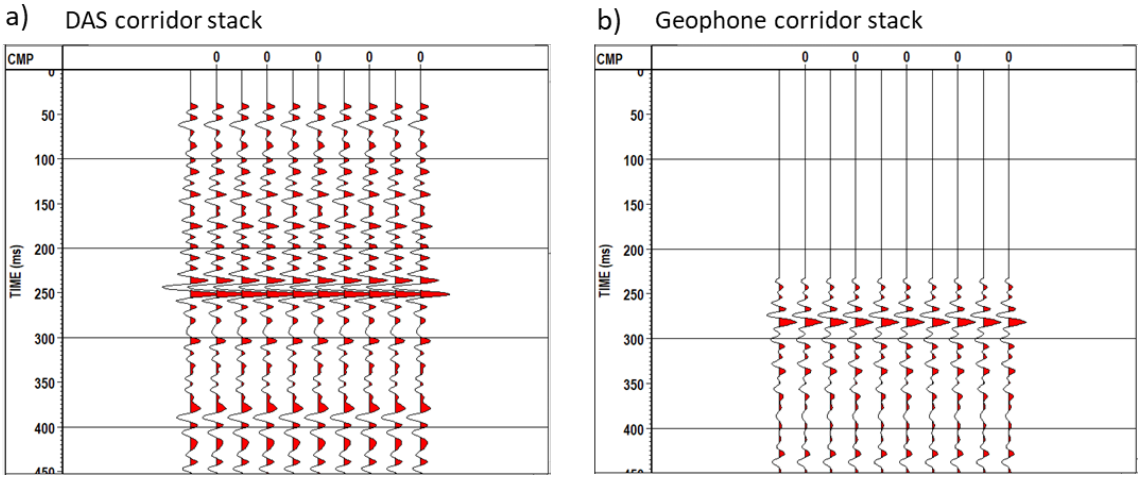

FIG. 20. Outside corridor Stack. Shot point 132, line 21, July 2017.

These same steps were applied for the fiber optic shot gathers and geophone shot gathers of the two zero offset source points from May and July and for the 80 m offset source point recorded in July. In the following section, the outside corridor stack and outside corridor stack mute are displayed for each shot point and data set mentioned above.

RESULTS

The following figures (21-38) correspond to the outside corridor stack and outside corridor stack mute obtained for both the fiber optic and geophone data sets of the shot points mentioned previously in Table 1.

Generally, there is a good match between the corridor stack of the upgoing and downgoing fibre loops side, as expected. Comparing this result with the geophone data set, it is noticeable a slight time difference for the high amplitude reflector corresponding to the reservoir. For example, for the zero-offset gathers, the high amplitude reflector is at approximately 250 ms in the fiber optic data set and at approximately 275 ms in the geophone array; and for the offset gather, the high amplitude reflector is at approximately 270 ms in the fiber optic data set and at approximately 290 ms in the geophone array.

Figures 39 to 41 show a combination of the two data sets for each shot point, where the similarities between the two sides of the fiber optic gather and the differences with the geophone data set mentioned above are more noticeable.

This difference might be caused due to the fact that each data set was recording a different measurement, the geophones record particle velocity and the fiber optic cable record Distributed Acoustic Sensing (DAS) measurements corresponding to strain. To compare DAS signal with geophone, one must convert from strain or strain-rate to particle velocity and take into account that, like ultrasonic transducers, radar antennas, or spatially distributed groups of geophones or hydrophones, the DAS signal intrinsically represents an integrated array response of conceptual point sensitivities (Miller et. al, 2016).

Few attempts to convert the DAS signal were performed with a function available in VISTA and after the calibration step mentioned previously, the difference between the first and last geophone was of 2 meters or 8 traces which is within the range of the results presented in the calibration segment. This conversion seems to be an interesting approach for a proper signal comparison. Nevertheless, a complete processing flow and a further analysis must be finished before having a concluding statement.

May 2017

DAS Zero offset VP: Line 13 shot 159 (left hand side)

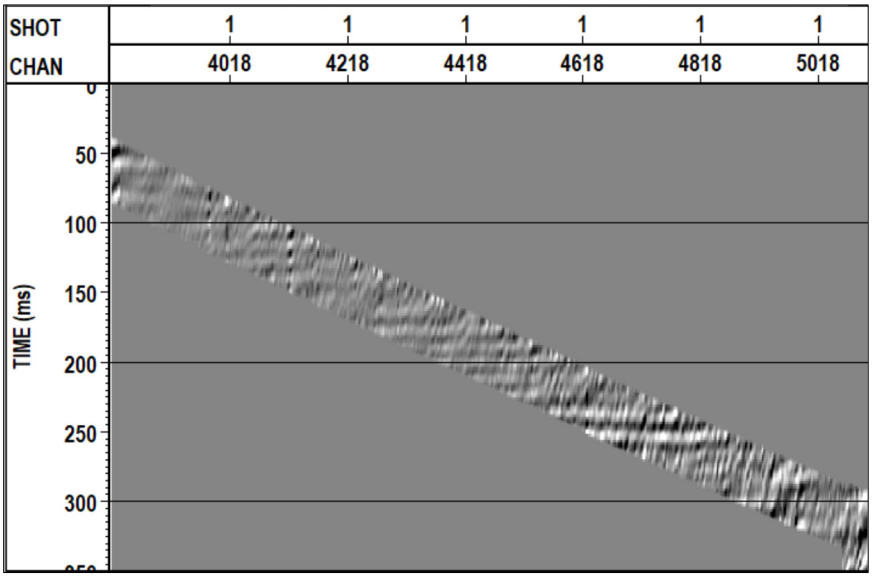

FIG. 21. Outside corridor stack mute. Shot 159, line 13, left hand side.

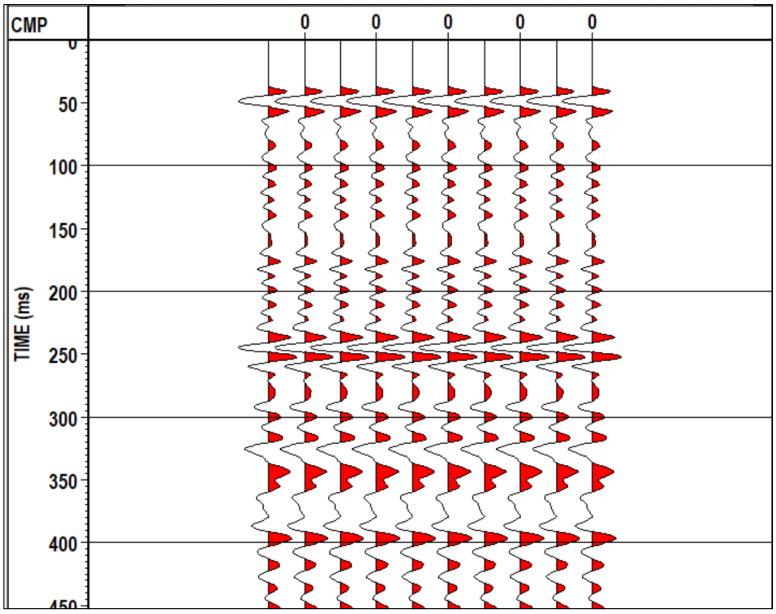

FIG. 22. Outside corridor stack. Shot 159, line 13, left hand side.

DAS Zero offset VP: Line 13 shot 159 (right hand side)

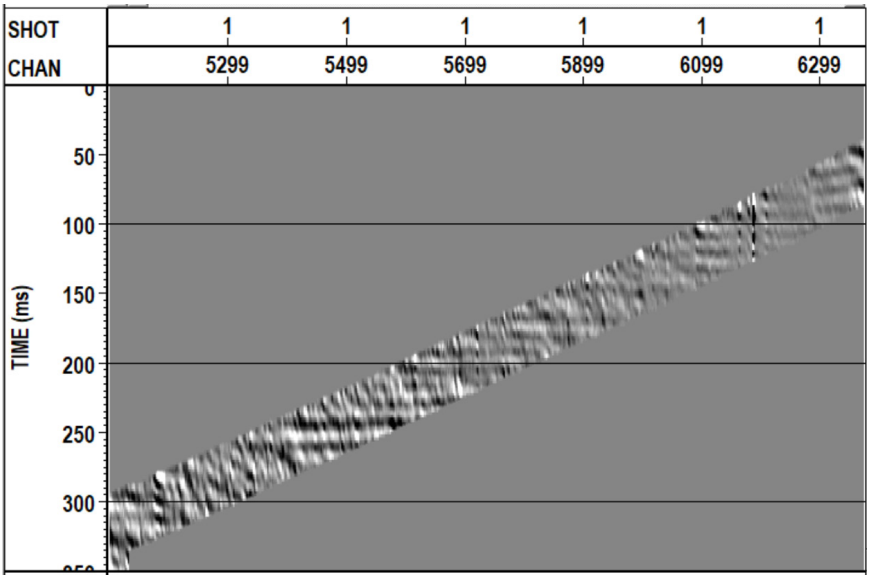

FIG. 23. Outside corridor stack mute. Shot 159, line 13, right hand side with 9bd.

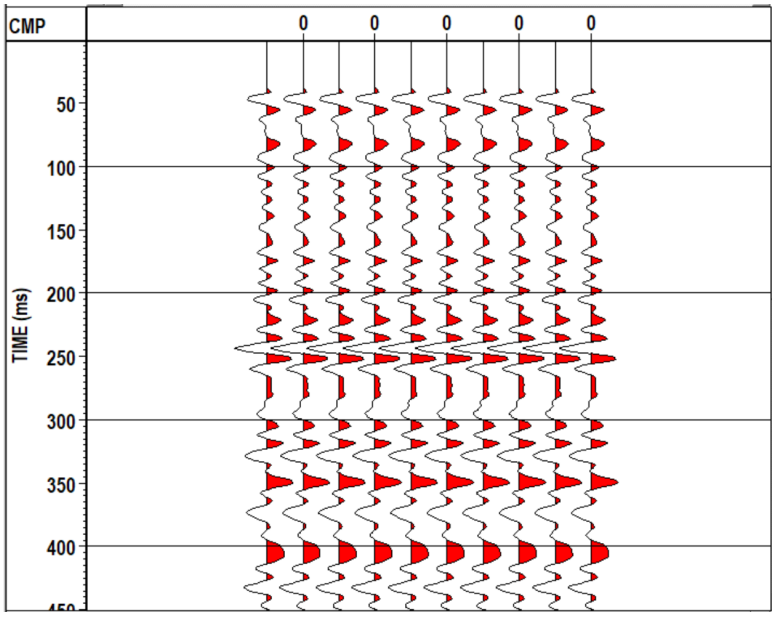

FIG. 24. Outside corridor stack. Shot 159, line 13, right hand side.

Geophones Zero offset VP: Line 13 shot 159

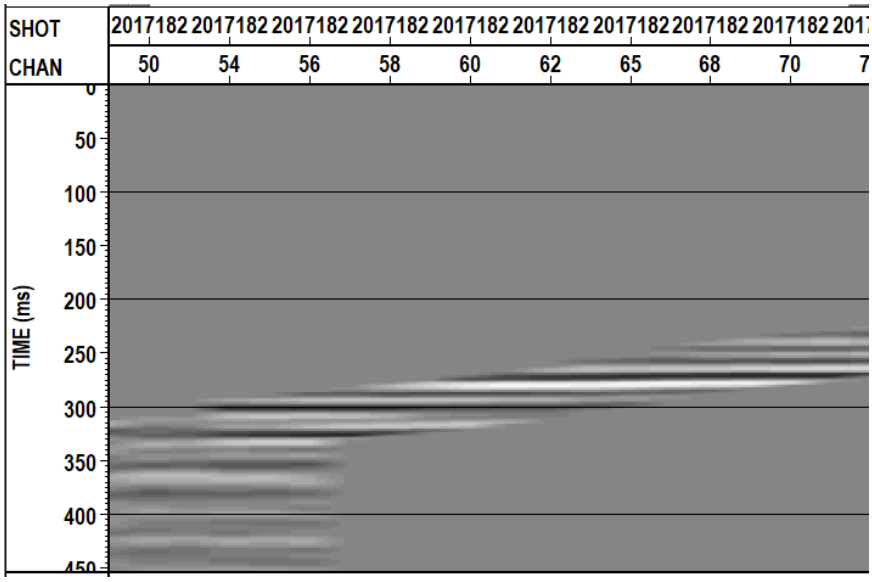

FIG. 25. Outside corridor stack mute. Shot 159, line 13.

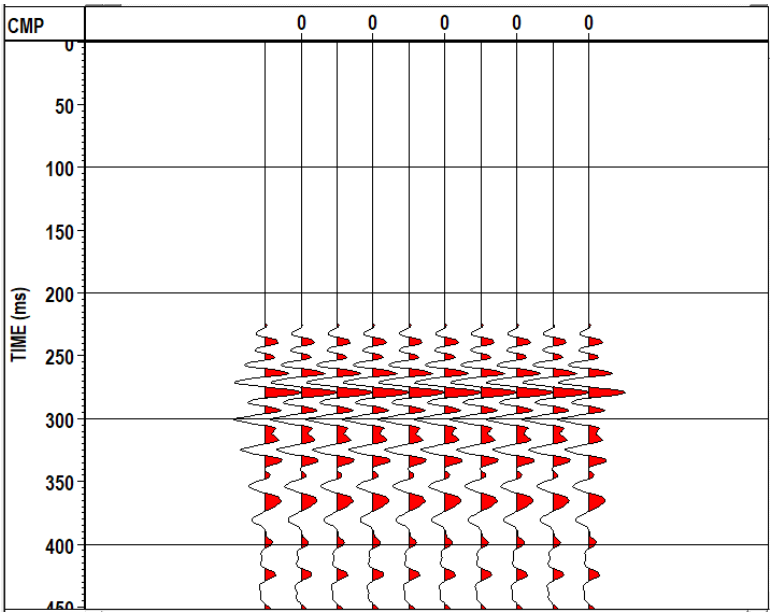

FIG. 26. Outside corridor stack. Shot 159, line 13.

July 2017

DAS Zero offset VP: Line 21 shot 132 left hand side

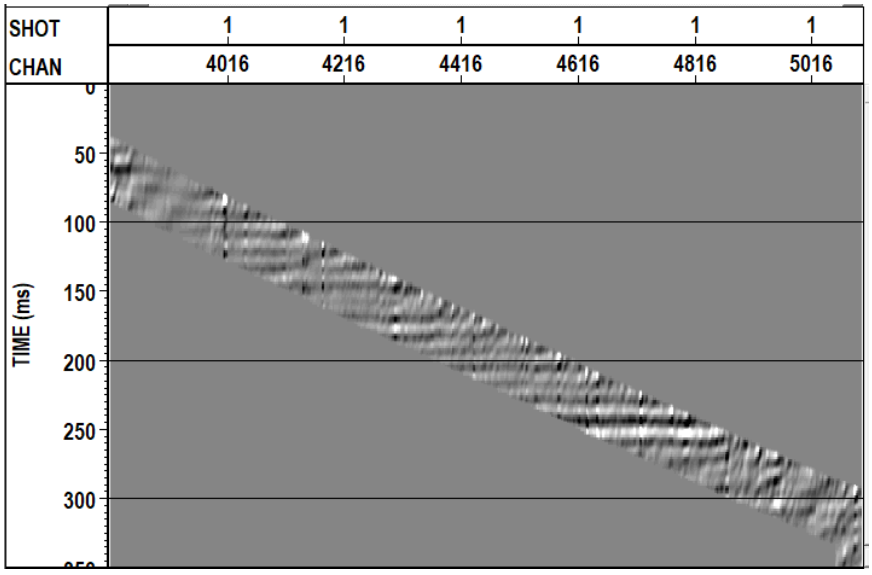

FIG. 27. Outside corridor stack mute. Shot 132, line 21, left hand side.

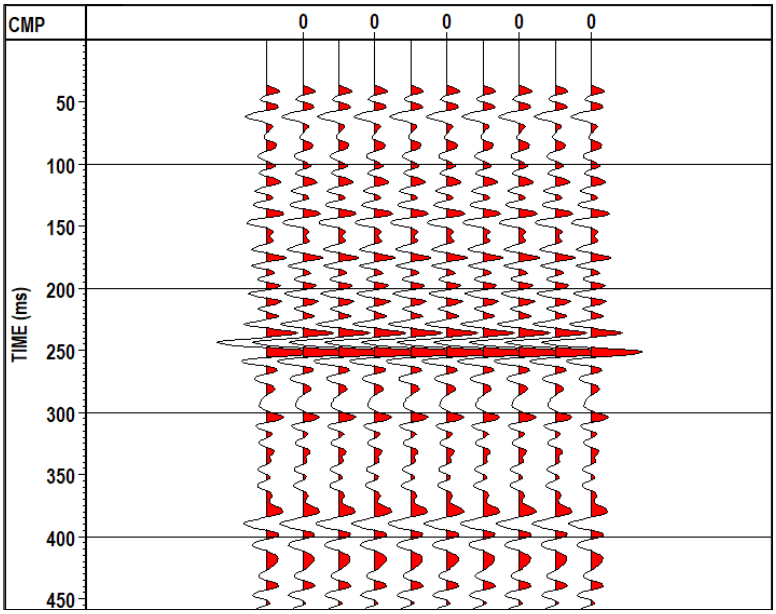

FIG. 28. Outside corridor stack. Shot 132, line 21, left hand side.

DAS Zero offset VP: Line 21 shot 132 right hand side

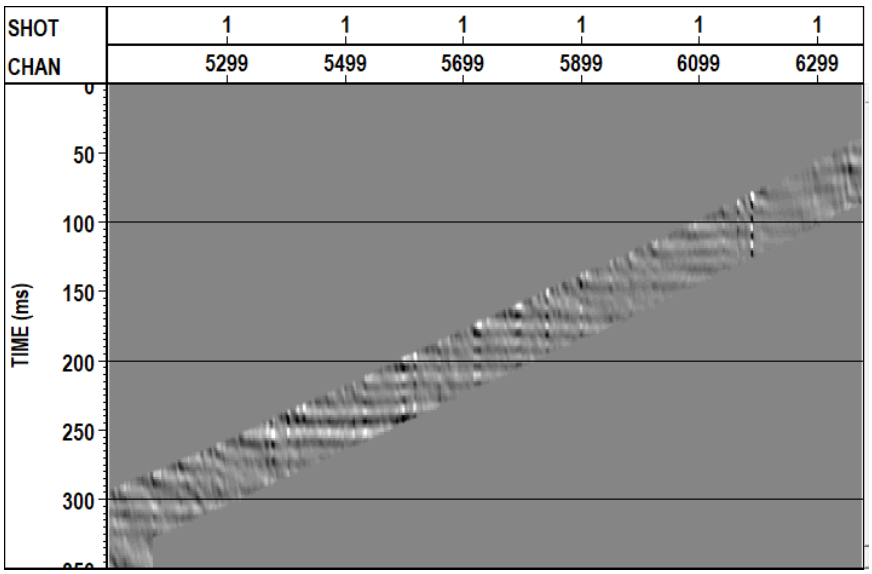

FIG. 29. Outside corridor stack mute. Shot 132, line 21, right hand side.

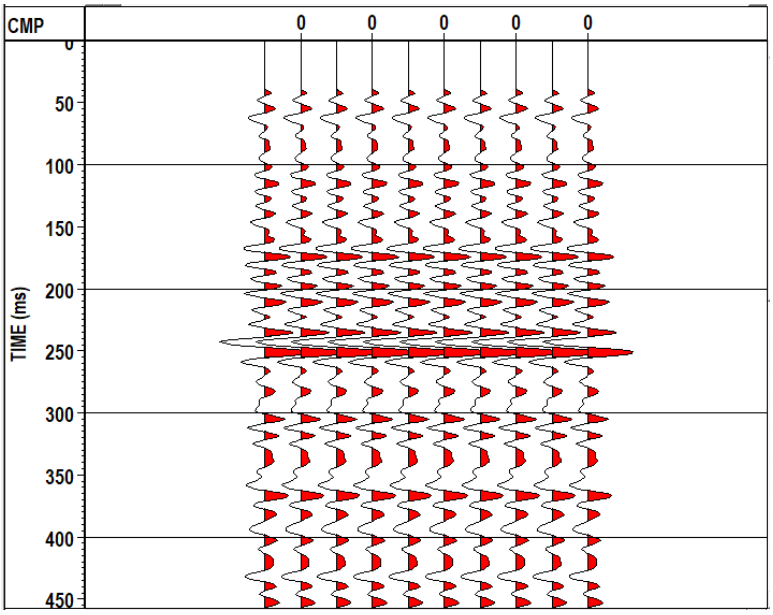

FIG. 30. Outside corridor stack. Shot 132, line 21, right hand side.

Geophones Zero offset VP: Line 21 shot 132

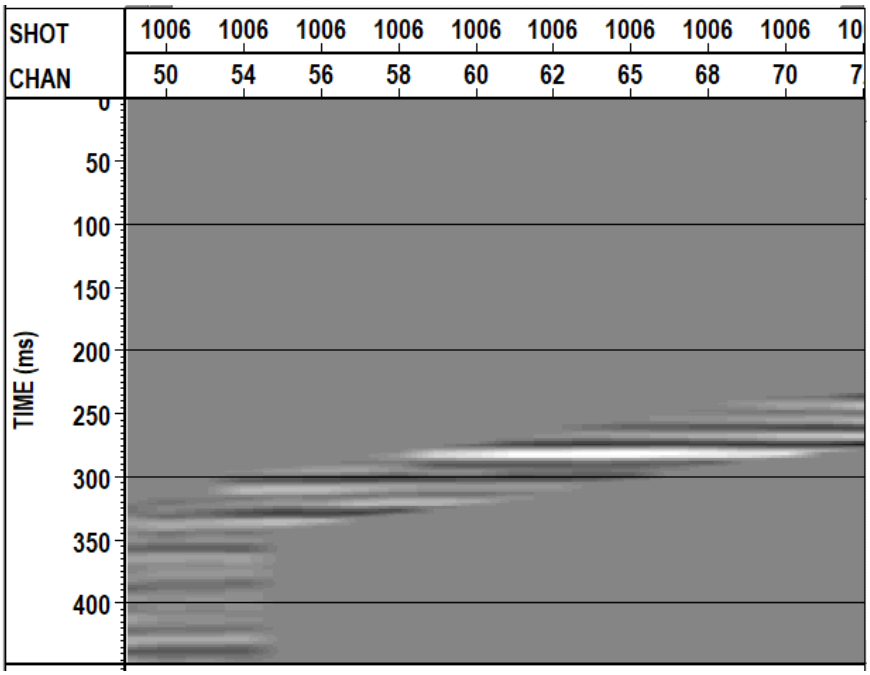

FIG. 31. Outside corridor stack mute. Shot 132, line 21.

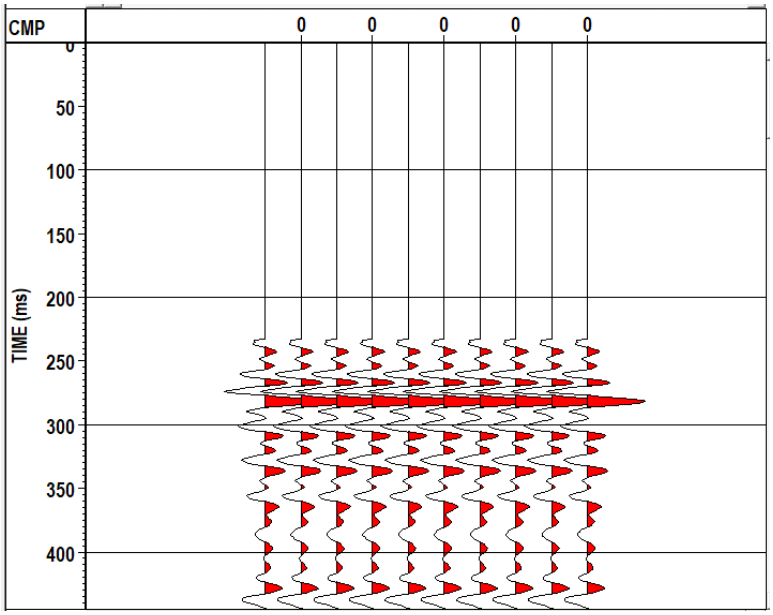

FIG. 32. Outside corridor stack. Shot 132, line 21.

DAS Offset VP: Line 21 shot 139 left hand side

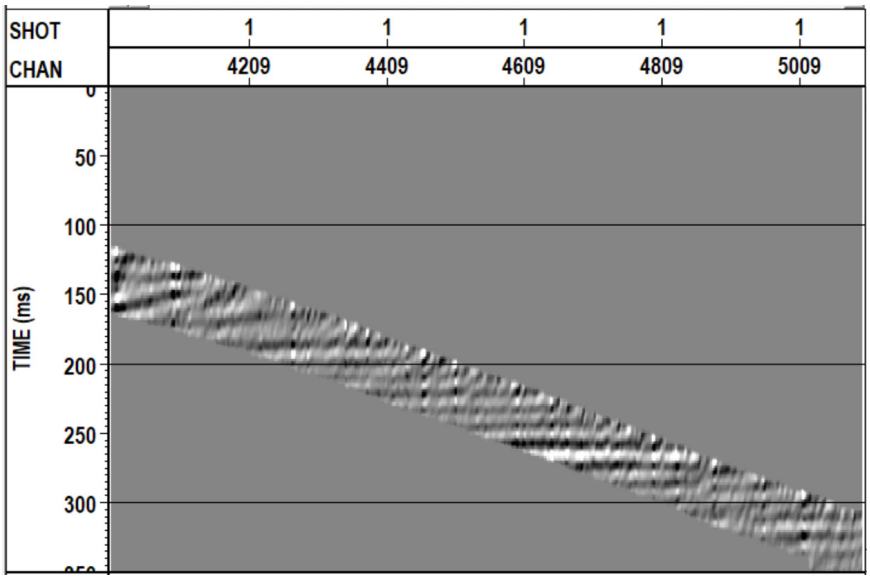

FIG. 33. Outside corridor stack mute. Shot 139, line 21, left hand side with 4db.

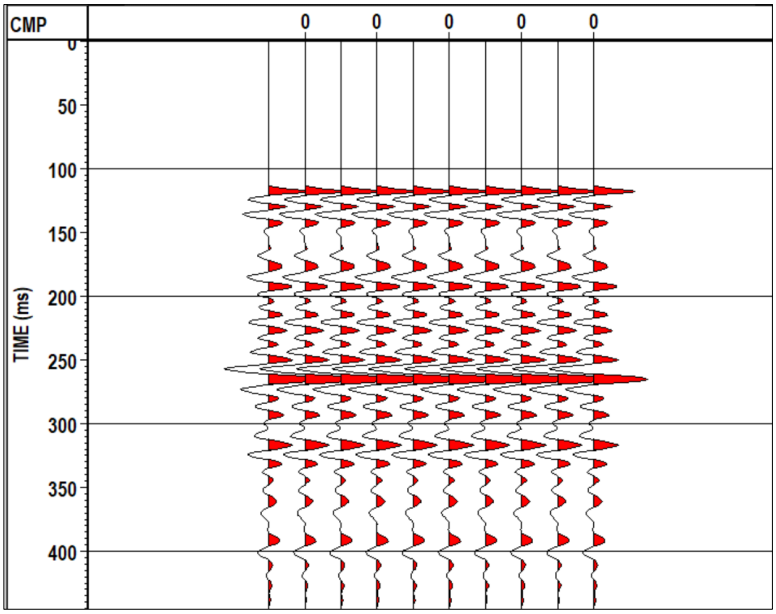

FIG. 34. Outside corridor stack. Shot 139, line 21, left hand side.

DAS Offset VP: Line 21 shot 139 right hand side

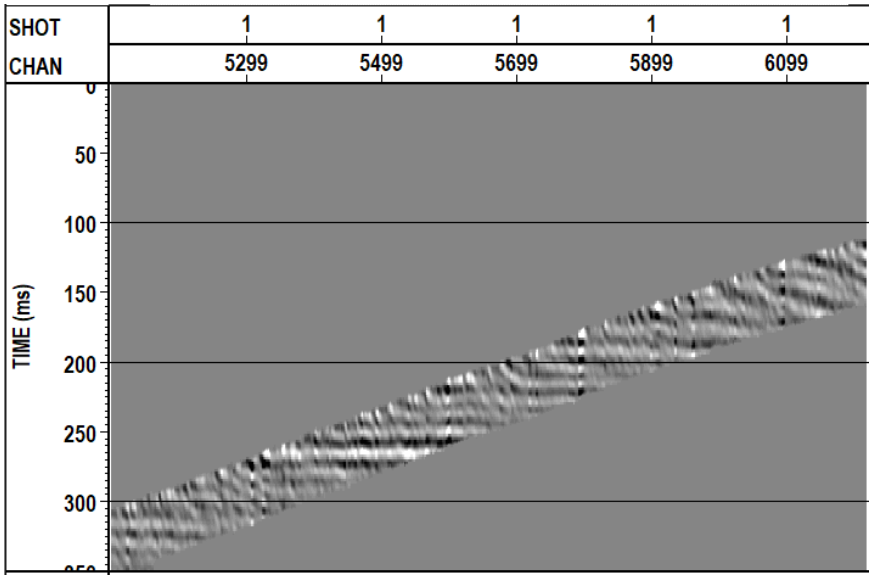

FIG. 35. Outside corridor stack mute. Shot 139, line 21, right hand side.

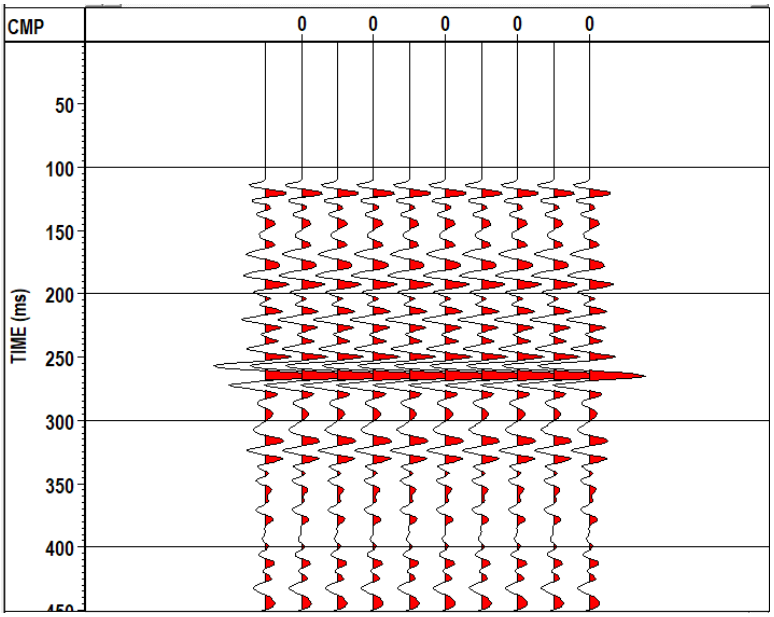

FIG. 36. Outside corridor stack. Shot 139, line 21, right hand side.

Geophones Offset VP: Line 21 shot 139

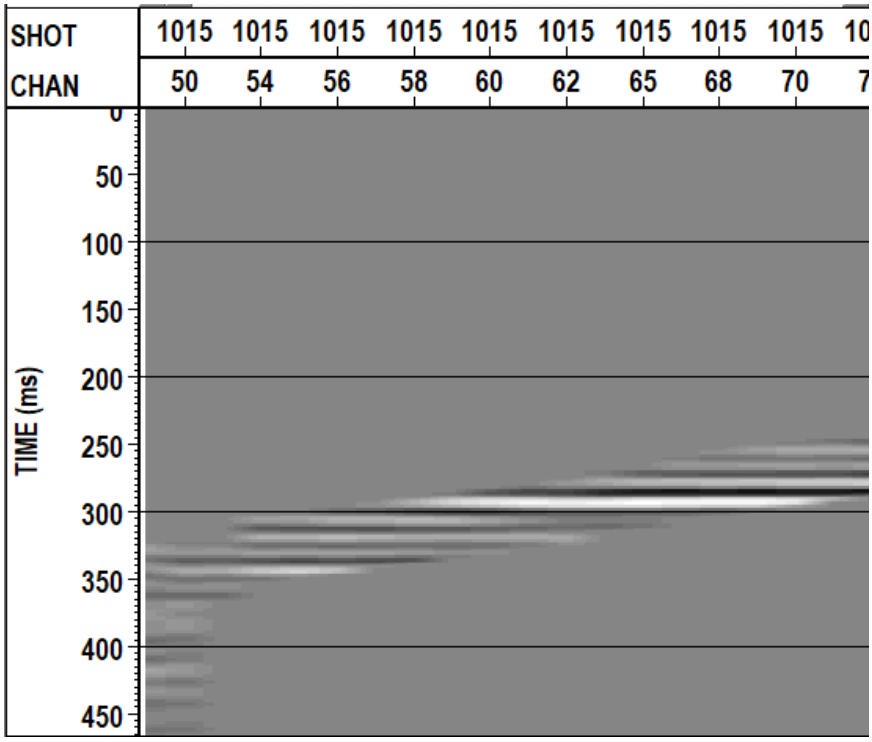

FIG. 37. Outside corridor stack mute. Shot 139, line 21.

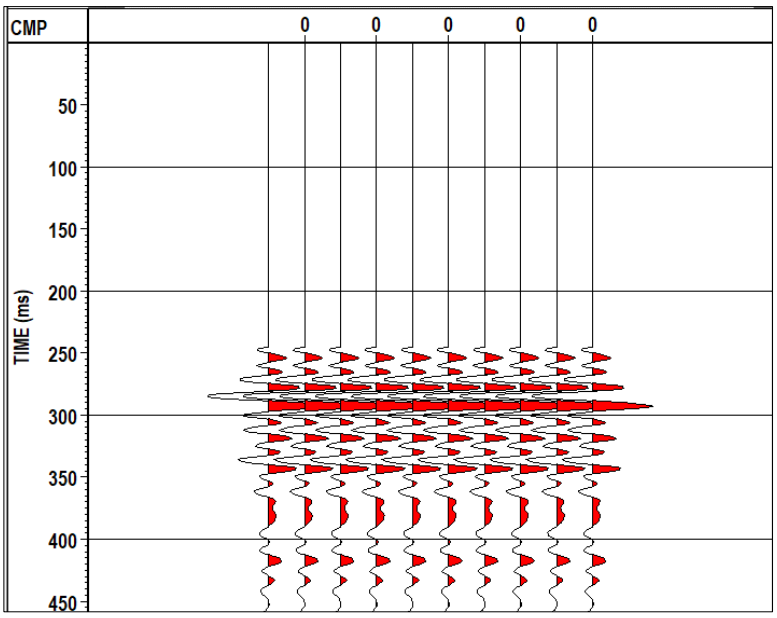

FIG. 38. Outside corridor stack. Shot 139, line 21.

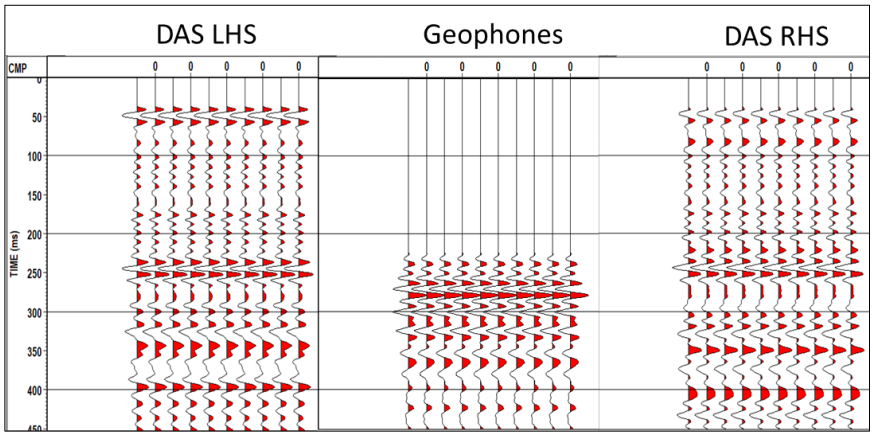

FIG. 39. Corridor stack comparison. Shot point 159, line 13, May 2017.

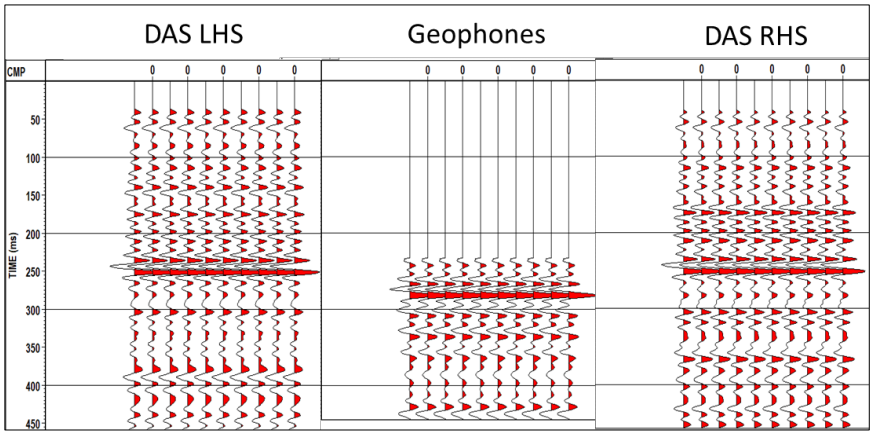

FIG. 40. Corridor stack comparison. Shot point 132, line 21, July 2017.

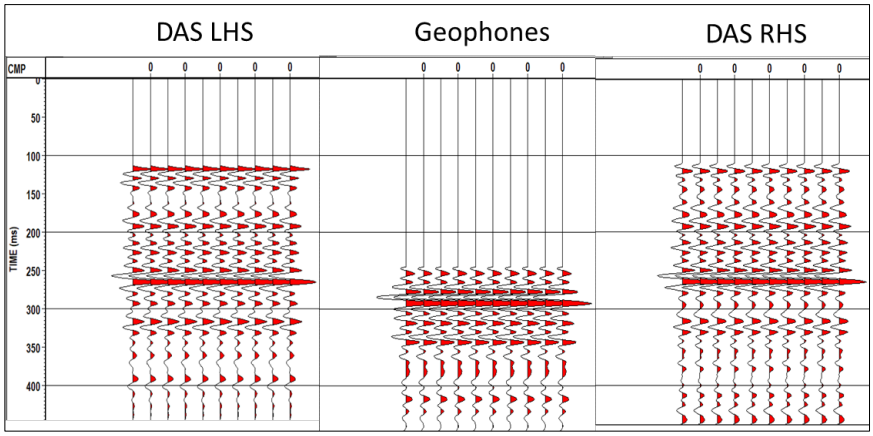

FIG. 41. Corridor stack comparison. Shot point 139, line 21, July 2017.

As a final comparison and quality control of these results, a cross-correlation of the fibre corridor stacks was performed for the shot point 132, line 21 from July 2017. Figure 42 shows the result of the cross-correlation. There is a good correlation between both sides as the maximum amplitude event is aligned at the zero-lag line. Several additional events are noticeable in the cross-correlation that might be cause to the difference between the first trace on each side of the loop or maybe could be artifacts generated during the cross-correlation, another possible cause are multiples. Further analysis is necessary to understand the cause of those events.

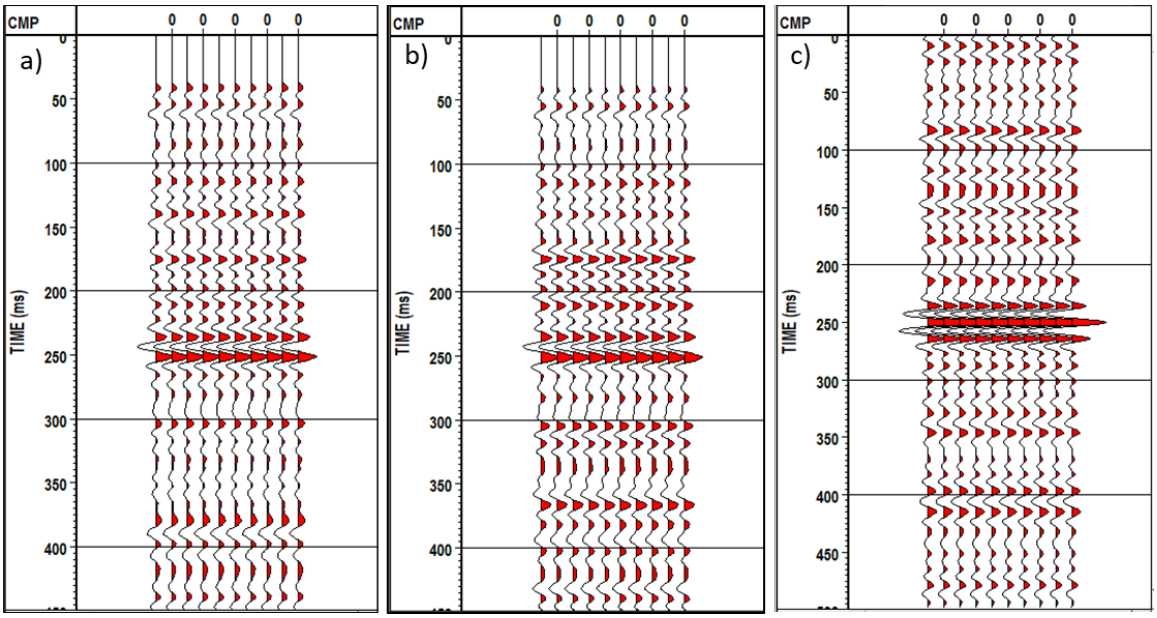

FIG. 42. Cross-correlation for fibre corridor stack of both sides of the fibre loop. a) left hand side fibre corridor stack, b) right hand side fibre corridor stack, c) cross-correlation result (250 ms zero-lag line).

CONCLUSIONS

Two VSP surveys were acquired at the Field Research Station in May and July, 2017 These surveys were acquired with a geophone array and a fiber optic (DAS) cable deployed in the observation well 2. Two zero-offset gathers and an 80 m source-well offset gather were processed using a standard processing flow.

The fiber optic data set was calibrated with the geophone array to properly identify the corresponding depth of each DAS trace. There was an accurate result between the cross-correlation of the first and last geophone trace, a difference between 0 to 3 m or 0 to 12 traces was calculated from the calibration.

As expected, there is a good match between the corridor stack of the upgoing and downgoing fibre loop. A time difference approximately of 20 ms between the DAS and geophone data is noticeable specially with the high amplitude reflector. This difference might be caused to the different signal measurements recorded by the geophones and the fiber optic cable.

Some tests to convert DAS signal into a similar geophone measurement were evaluated. The calibration difference between the first and last geophone after the conversion was similar to the previous results. The converted signal needs to be processed completely in order to do a proper comparison with the results shown in this report.

FUTURE WORK

These results encourage a more detailed velocity model analysis obtained from the first break times and the culmination of the processing flow for the walk-away VSP surveys acquired in May and July 2017 using fiber optic cables and geophones for imaging purposes. Compare the results obtained between the two data sets.

Continue the DAS signal conversion in order to retrieve a more precise comparison between the signal recorded with the fiber optic cable and the geophone array.

Process the helical-wound fiber optic data set and compare it with the horizontal components of the geophone data set.

ACKNOWLEDGEMENTS

We would like to thank CREWES sponsors and NSERC (Natural Science and Engineering Research Council of Canada) support through the grant CRDPJ 461179-13. We also thank the Containment and Monitoring Institute (CaMI) for the opportunity to develop this research. Further thanks to Dr. Marie Macquet and Dr. Raul Cova for their guidance and discussions during this research.

REFERENCES

Bubshait, S.,2010, VSP processing for coal reflections. Calgary: University of Calgary.

Lawton, D. C., 2017, Monitoring technology innovation at the CaMI Field Research Station, Brooks, Alberta. Calgary: CMC.

Mateeva A., Lopez J., Potters H., Mestayer J., Cox B., Kiyashchenko D., Wills P., Grandi S., Hornman K., Kuvshinov B., Berlang W., Yang Z. and Demoto R., 2014, Distributed acoustic sensing for reservoir monitoring with vertical seismic profiling. Geophysical Prospecting, 679-692.

Miller D. E., Daley T. M., White D., Freifeld B. M., Robertson M., Cocker J. and Craven M., 2016, Simultaneous Acquisition of Distributed Acoustic Sensing VSP with Multi-mode and Singlemode Fibre Optic Cables and 3C Geophones at the Aquistore CO2 Storage Site. Recorder.

Parker T., Shatalin S. and Farhadiroushan M., 2014, Distributed Acoustic Sensing – a new tool for seismic applications. First Break, 61-69.

Wu H., Wong W.,Yang Z., Wills P. B., Lopez J., Li Y., Blonk B., Hewett B. and Mateeva A., 2015, Dual-well 3D vertical seismic profile enabled by distributed acoustic. Interpretration, SW12--SW25.